AUTOMATED DELINEATION OF ROOF PLANES FROM LIDAR DATA

F. Rottensteiner [a], *, J. Trinder [b], S. Clode [c], K. Kubik [c]

[a] Institute of Photogrammetry and Remote Sensing, Vienna University of Technology,
Gußhausstraße 27-29, 1040 Vienna, Austria - fr@ipf.tuwien.ac.at
[b] School of Surveying and Spatial Information System, The University of New South Wales,
UNSW SYDNEY NSW 2052, Australia – j.trinder@unsw.edu.au
[c] The Intelligent Real-Time Imaging and Sensing Group, School of ITEE, The University of Queensland,
Brisbane QLD 4072, Australia – (sclode, kubik)@itee.uq.edu.au

Commission III, WG III/4

KEY WORDS: Building reconstruction, laser scanning, step edge detection, 3D city models

ABSTRACT:

In this paper, we describe an algorithm for roof line delineation from LIDAR data which aims at achieving models of a high level of detail. Roof planes are initially extracted by segmentation based on the local homogeneity of surface normal vectors of a digital surface model (DSM). A case analysis then reveals which of these roof planes intersect and which of them are separated by a step edge. The positions of the step edges are determined precisely by a new algorithm taking into account domain specific information. Finally, all step edges and intersection lines are combined to form consistent polyhedral models. In all phases of this workflow, decision making is based upon statistical reasoning about geometrical relations between neighbouring entities in order to reduce the number of control parameters and to increase the robustness of the method.

1. INTRODUCTION

1.1 Motivation and Goals

LIDAR data offer a high potential for automated building extraction. Buildings consist of regular surfaces that can be extracted from LIDAR data making use of surface properties such as local co-planarity. One approach to reconstruct buildings from LIDAR data is to segment the data into planes and then to combine these planes to obtain a polyhedral model (Vosselman, 1999; Vögtle & Steinle, 2000; Rottensteiner, 2003; Alharty & Bethel, 2004). Alternatively, buildings can be reconstructed by parametric primitives, e.g. (Brenner, 2000). Using parametric primitives reduces the level of detail that can be achieved as the number of primitives is usually small and most have a rectangular footprint. The greatest problem encountered with generic methods for reconstructing polyhedral models is the delineation of the roof plane boundaries. These boundaries correspond to edges in the LIDAR data. In contrast to edges corresponding to the intersection of neighbouring roof planes that can be determined very precisely, step edges are poorly defined. As step edges occur at building outlines, 2D GIS data are often used in combination with LIDAR data to alleviate this problem, e.g. (Brenner, 2000).

If no GIS data are available, the roof boundaries have to be determined from edges extracted from the LIDAR data. The approximate positions of such edges are given by the boundaries of the planar segments that have been extracted from a Digital Surface Model (DSM) created from the LIDAR data. As these positions are not very precise, the determined polygons appear very ragged and regularisation techniques need to be applied. Some algorithms rely on assumptions with respect to the roof shapes, e.g. on all corners being right-angled

(Vosselman, 1999), which reduces the level of detail of the resulting models. Another common feature of such algorithms is that they rely on comparing distances to user-defined thresholds for taking decisions regarding geometric constraints. Of course, the setting of such thresholds is a critical issue. Another problem is that the quality of the outlines of the planar segments will also tend to be poor in areas where other objects occlude parts of the roof planes (Alharty & Bethel, 2004).

The goal of this paper is twofold. First, we want to describe a method for roof plane delineation that eliminates user-defined thresholds as far as possible. This is achieved by making all decisions dependent on statistical reasoning, relying on the framework of uncertain projective geometry (Heuel, 2004) and on robust estimation (Kager, 1989). Second, we want to describe a new algorithm for the detection of step edges for delineating roof polygons, taking into account domain specific information in order to eliminate disturbances caused by trees adjacent to buildings.

1.2 Related Work

Vosselman (1999) described a method for the reconstruction of buildings by polyhedral models from LIDAR data. His algorithm for planar segmentation operates on a Delaunay triangulation of the original LIDAR points. The initial roof boundaries are given by the edges of the outmost triangles of the roof planes. Two planes are considered to intersect if the distance between their outlines is small. Step edges are assumed to be either parallel or orthogonal to the main direction of the building, and a merging algorithm is used to obtain sequences of boundary points belonging to the same straight line segment. By these assumptions, the algorithm is restricted to buildings only having right-angled corners at their outlines.

---

* Corresponding author.

Vögtle and Steinle (2000) determine step edges as roof plane outlines of significant elevation difference and estimate the position of these edges by an adjustment procedure taking into account the maximum gradient of the DSM in the vicinity of the edge. The authors do not describe how they determine the shapes of more complex step edges. Relying on the maximum gradient of the DSM is critical at building outlines. This is also acknowledged by Alharty and Bethel (2004). They thin out the initial roof boundary polygons derived from the outlines of the planes by subsequently eliminating points that are determined not to contribute significantly to the polygon. This results in isolated polygons for each roof plane, which are not necessarily connected. Neighbouring polygon segments are aligned if their 2D distance is below a threshold, and vertices are merged if their 3D distance is small. No adjustment of the vertices is carried out apart from computing their average position.

Sze et al. (1998) and Jiang and Bunke (1999) described edge extraction algorithms from range images. These algorithms detect edges at discontinuities of both height and slope. In the context of building reconstruction, step edges extracted by a generic edge extractor would have to be matched with the approximate roof outlines. In the case of trees adjacent to buildings, the edge extractor is likely to determine the outline of the trees rather than the building outline. In (Rottensteiner, 2003), it was shown how planes can be detected in a LIDAR DSM. Edge pixel candidates were determined at positions of maximum height gradient. Again, this resulted in problems where trees were adjacent to buildings. In order to overcome such problems, we propose to use a specific step edge extraction technique that takes into account domain specific information for detecting edge candidate pixels.

2. BACKGROUND

2.1 Workflow for Automated Building Reconstruction

In this work, we assume the locations of buildings to be known. We use the algorithm described in (Rottensteiner et al., 2004) for building detection. The building outlines are only known with an accuracy of up to 1-3 m. The accuracy of the LIDAR point is given by the standard deviations σ_P and σ_Z of a planimetric co-ordinate and the height. We chose $\sigma_P = \pm 25$ cm and $\sigma_Z = \pm 7.5$ cm. First, the LIDAR data are sampled into a DSM in the form of a regular grid of width Δ by linear prediction. For the examples in this paper, the point spacing of the LIDAR data was 1.2 m, and we chose $\Delta = 0.5$ m. The work flow for the geometric reconstruction of buildings consists of four steps:

1. **Detection of roof planes** based on a segmentation of the DSM to find planes which are expanded by region growing.
2. **Grouping of roof planes and roof plane delineation:** Co-planar roof segments are merged, and hypotheses for intersection lines and/or step edges are created based on an analysis of the neighbourhood relations.
3. **Consistent estimation of the building parameters** to improve these parameters using all available sensor data.
4. **Model regularisation** by introducing hypotheses about geometric constraints into the estimation process.

In this paper we will focus on the second stage, describing a new algorithm for step edge detection and showing how statistical tests and robust estimation can be applied to make decisions in the reconstruction process.

2.2 Representation of Geometric Entities

In this work, we represent geometric entities by their homogeneous co-ordinates and by the variance-covariance matrices of these co-ordinates (Heuel, 2004). Each vector consists of a homogeneous part and Euclidean part; a Euclidean representation (which is essentially required for graphical output) can be achieved by dividing the vector by the norm of the homogeneous part. The variance-covariance matrix of the Euclidean representation can be derived by error propagation. To avoid numerical problems, the centre of the co-ordinate system is shifted to the centre of the building.

- With 2D and 3D points, we generally use the Euclidean representation: $\mathbf{X}^{2D} = (X,Y,1)^T$ and $\mathbf{X}^{3D} = (X,Y,Z,1)^T$. For the variance-covariance matrix $\mathbf{Q}_X$ of the LIDAR points we assume $q_{XY} = q_{XZ} = q_{YZ} = 0$, $q_{XX} = q_{YY} = \sigma_P^2$ and $q_{ZZ} = \sigma_Z^2$.
- 2D lines are represented by $\mathbf{L}^{2D} = (A\ B\ W)^T$, where the homogeneous part $(A\ B)^T$ is the normal vector of the line. The rank of the variance-covariance matrix $\mathbf{Q}_{L2D}$ is 2. 2D edge segments, i.e. polygon segments at step edges, are represented by $\mathbf{L}_{2D}$, $\mathbf{Q}_{S2D}$, their endpoints $\mathbf{X}^{2D}_1$ and $\mathbf{X}^{2D}_2$, and their centre point $\mathbf{X}^{2D}_C$. $\mathbf{L}^{2D}$ and $\mathbf{Q}_{L2D}$ are estimated from the edge candidate points assigned to the edge segments by minimising the squared sum of the distances of these points from the line.
- 3D planes are represented by vectors $\mathbf{P} = (A\ B\ C\ W)^T$, where the homogeneous part $(A\ B\ C)^T$ is the normal vector of the plane. The rank of the variance-covariance matrix $\mathbf{Q}_P$ is 3. We also store the centre point $\mathbf{X}^{3D}_C$ of the plane. $\mathbf{P}$ and $\mathbf{Q}_P$ are estimated from the DSM points assigned to the plane by minimising the squared sum of the distances of these points from the plane.
- 3D lines are represented by vectors $\mathbf{L}_{3D} = (L_1\ L_2\ L_3\ L_4\ L_5\ L_6)^T$, where the homogeneous part $(L_1\ L_2\ L_3)^T$ is the directional vector of the line. If the line is constructed from two points $\mathbf{X}^{3D}_1$ and $\mathbf{X}^{3D}_2$, the vector $(L_4\ L_5\ L_6)^T$ can be interpreted as the cross-product of $\mathbf{X}^{3D}_1$ and $\mathbf{X}^{3D}_2$. The rank of the variance-covariance matrix $\mathbf{Q}_{L3D}$ is 4. 3D edge segments are represented by $\mathbf{L}_{3D}$, $\mathbf{Q}_{L3D}$, and their endpoints $\mathbf{X}^{3D}_1$ and $\mathbf{X}^{3D}_2$. $\mathbf{L}_{3D}$ and $\mathbf{Q}_{S3D}$ are derived by the intersection of two planes.

2.3 Testing of Geometric Relations

In order to test whether two geometric entities $\mathbf{N}$ and $\mathbf{M}$ fulfil a certain geometric relation, a distance metric $\mathbf{d}_{NM}$ and its variance-covariance matrix $\mathbf{Q}_{NM}$ can be computed:

$$\mathbf{d}_{NM} = \mathbf{A}(\mathbf{N}) \cdot \mathbf{M} = \mathbf{B}(\mathbf{M}) \cdot \mathbf{N}$$

$$\mathbf{Q}_{NM} = \mathbf{A}(\mathbf{N}) \cdot \mathbf{Q}_M \cdot \mathbf{A}^T(\mathbf{N}) + \mathbf{B}(\mathbf{M}) \cdot \mathbf{Q}_N \cdot \mathbf{B}^T(\mathbf{M}) \tag{1}$$

Relation	N	M	A(N)	B(N)	dof
Identity	$\mathbf{L}^{2D}_1$	$\mathbf{L}^{2D}_2$	$\mathbf{S}(\mathbf{L}^{2D}_1)$	$-\mathbf{S}(\mathbf{L}^{2D}_2)$	2
Incidence	$\mathbf{X}^{3D}$	$\mathbf{P}$	$\mathbf{X}^{3D\ T}$	$\mathbf{P}^T$	1
Incidence	$\mathbf{L}^{3D}$	$\mathbf{X}^{3D}$	$\overline{\Gamma}^T(\mathbf{L}^{3D})$	$\overline{\Pi}^T(\mathbf{X}^{3D})$	2
Incidence	$\mathbf{L}^{3D}_1$	$\mathbf{L}^{3D}_2$	$\overline{\mathbf{S}}^{1\ T}_{3D}$	$\overline{\mathbf{S}}^{2\ T}_{3D}$	1

Table 1. Definitions of the matrices **A** and **B** in equation 1 (Heuel, 2004). *dof*: Degrees of freedom of the test.

In equation 1, $\mathbf{A}(\mathbf{N})$ and $\mathbf{B}(\mathbf{M})$ are matrices depending on $\mathbf{N}$ and $\mathbf{M}$, respectively. Table 1 sums up the definitions of **A** and **B** for the relations that are of interest in the context of our work. The definitions of the construction matrices used in table 1 are given by equations 2 (Heuel, 2004).

$$\overline{\Pi}\left(\mathbf{X}^{3D}\right) = \begin{pmatrix} 0 & -Z & Y & 0 \\ Z & 0 & -X & 0 \\ -Y & X & 0 & 0 \\ 1 & 0 & 0 & -X \\ 0 & 1 & 0 & -Y \\ 0 & 0 & 1 & -Z \end{pmatrix} \qquad \mathbf{S}\left(\mathbf{X}^{2D}\right) = \begin{pmatrix} 0 & -1 & Y \\ 1 & 0 & -X \\ -Y & X & 0 \end{pmatrix}$$

$$\overline{\Gamma}\left(\mathbf{L}^{3D}\right) = \begin{pmatrix} 0 & L_3 & -L_2 & -L_4 \\ -L_3 & 0 & L_1 & -L_5 \\ L_2 & -L_1 & 0 & -L_6 \\ L_4 & L_5 & L_6 & 0 \end{pmatrix} \qquad (2)$$

The dimension of the distance vector $\mathbf{d}_{NM}$ according to table 1 and equations 1 and 2 might be higher than the degree of freedom (dof) of the test, resulting in a singular variance-covariance matrix $\mathbf{Q}_{NM}$. Thus, dof rows of $\mathbf{A(N)}$ and $\mathbf{B(M)}$ have to be selected in order to obtain a reduced distance vector $\mathbf{d}'_{MN}$:

$$\mathbf{d}'_{NM} = \mathbf{A}'(\mathbf{N}) \cdot \mathbf{M} = \mathbf{B}'(\mathbf{M}) \cdot \mathbf{N}$$
$$\mathbf{Q}'_{NM} = \mathbf{A}'(\mathbf{N}) \cdot \mathbf{Q}_M \cdot \mathbf{A}'^T(\mathbf{N}) + \mathbf{B}'(\mathbf{M}) \cdot \mathbf{Q}_N \cdot \mathbf{B}'^T(\mathbf{M})$$

$$(3)$$

$\mathbf{A}'$ and $\mathbf{B}'$ are the reduced matrices. From $\mathbf{d}'_{NM}$, a quantity t_{MN} following a χ^2_{dof} distribution can be derived:

$$t_{NM} = \mathbf{d}'^T_{MN} \cdot Q'^{-1}_{MN} \cdot \mathbf{d}'_{MN} \qquad (4)$$

Using a significance level α, a hypothesis is accepted if t_{MN} is smaller than the $(1-\alpha)$ - quantile $\chi^2_{1-a;\, dof}$ of the χ^2_{dof} distribution with dof degrees of freedom. Hypotheses H_i about geometrical relations can be ranked according to the ratios between the test statistics t'_{MN} and the quantiles $\chi^2_{1-a;\, dof(i)}$.

3. ROOF PLANE DELINEATION

3.1 Detection of Roof Planes

For roof plane detection we use the iterative scheme of seed region detection and region growing described in (Rottensteiner, 2003). In region growing, each point $\mathbf{X}^{3D}$ of the DSM adjacent to the seed region has to be tested whether or not it belongs to the plane $\mathbf{P}$. In order to speed up the computation, the variance σ^2_d of the distance of $\mathbf{X}^{3D}$ from $\mathbf{P}$ is computed only once for a fixed point at a certain distance from $\mathbf{P}$'s centre point $\mathbf{X}^{3D}_C$, so that in the region growing process the distance of each point has to be compared to a fixed threshold d_{max}:

$$d_{\max} = \sqrt{\chi^2_{1-\alpha;1}} \cdot \sigma_d \qquad (5)$$

This is justified by the fact that σ^2_d is dominated by the uncertainty of $\mathbf{X}^{3D}$ and the Euclidean part of $\mathbf{P}$. After each iteration, the roof plane parameters are recomputed and a decision on whether or not a detected segment actually corresponds to a plane. This is done by comparing the r.m.s. error σ_0 of unit weight of the planar adjustment to a user-defined threshold σ_{Pmax}. It could, however, be replaced by a test of σ_0, comparing it to the accuracy of a LIDAR point. Here, we choose $\sigma_{Pmax} = 2 \cdot \sigma_Z$.

Our iterative scheme of seed region selection and region growing yields an oversegmentation of the DSM (Rottensteiner, 2003). Co-planar neighbouring planes have to be merged after segmentation. For each pair of neighbouring planes $\mathbf{P}_i$ and $\mathbf{P}_j$ we compute the parameters of the combined plane as well as its r.m.s. error of unit weight σ_c. The ratio $F = \sigma^2_c / \sigma^2_s$ between σ_c and the r.m.s. error of unit weight σ_s of a separate adjustment of the two planes follows a Fisher distribution with $f_c = n_i + n_j - 3$

and $f_s = n_i + n_j - 6$ degrees of freedom, where n_i and n_j are the numbers of DSM points assigned to $\mathbf{P}_i$ and $\mathbf{P}_j$, respectively. In order to compare hypotheses about the co-planarity of planes, we compute the ratio $r_{ij} = F / F_{fc,\, fs,1-\alpha} = \sigma^2_c / (\sigma^2_s \cdot F_{fc,\, fs,1-\alpha})$, where $F_{fc,\, fs,1-\alpha}$ is the $(1-\alpha)$ - quantile of the Fisher distribution. Two planes $\mathbf{P}_i$ and $\mathbf{P}_j$ are considered to be co-planar if $r_{ij} < 1$. As this turned out to be too pessimistic, we introduced a second criterion, accepting planes to be co-planar if σ_c is below a certain threshold. All co-planar pairs $\mathbf{P}_i$ and $\mathbf{P}_j$ are ranked according to r_{ij}. The pair receiving the minimum value of r_{ij} is merged, and the co-planarity ratios r_{ij} are re-computed for the remaining planes. This process is repeated until no further planes can be merged. The upper part of Figure 1 shows the planar segmentation for a simple roof partly occluded by trees, whilst the lower part shows a more complex industrial building.
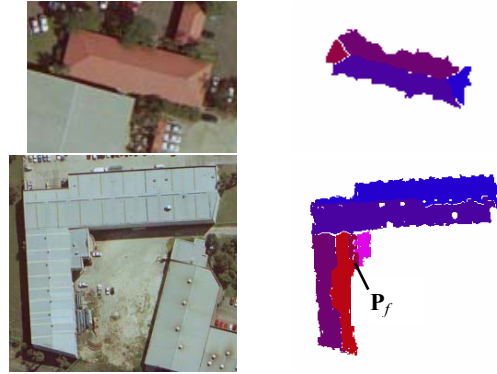

Figure 1. Orthophoto (left) and planar segments (right) for two buildings. Width of upper window: 60 m; lower window: 115 m. Plane $\mathbf{P}_f$ will be eliminated later.

3.2 Classification of Neighbourhood Relations

Once the roof planes have been detected, their boundary polygons are determined. We create a Voronoi diagram of the planar segments. The boundaries of the planes $\mathbf{P}_i$ in the Voronoi diagram deliver approximate values for the boundary polygons p_i of these planes. By using the Voronoi diagram for approximations, we overcome segmentation problems such as gaps between neighbouring planes (e.g. caused by chimneys), or incomplete planes due to occluding trees. The heights of the vertices of p_i are computed using the parameters of the plane $\mathbf{P}_i$. The polygons p_i are split into an ordered set of polygon segments $p_{i,j,k}$, where each segment $p_{i,j,k}$ separates plane $\mathbf{P}_i$ from its neighbouring plane $\mathbf{P}_j$. (The index k refers to the sequential position of $p_{i,j,k}$ within p_i, whereas the index j denotes the neighbouring plane. Unlike j, k can thus only occur once in p_i). Then, each polygon segment $p_{i,j,k}$ is classified according to whether it corresponds to a step edge or to an intersection line. This classification has to take into account the uncertainty of the planes $\mathbf{P}_i$ and $\mathbf{P}_j$ and of the approximate positions of the vertices $\mathbf{X}^l_{i,j,k}$ of $p_{i,j,k}$. We test all vertices of $p_{i,j,k}$ whether they are co-incident with the intersection line $\mathbf{L}^{3D}$ of $\mathbf{P}_i$ and $\mathbf{P}_j$, in the way described in section 2.3. The standard deviation of a planimetric co-ordinate σ_P of $\mathbf{X}^l_{i,j,k}$ has to reflect the fact that the boundaries of the Voronoi diagram are more uncertain for roofs having a small tilt δ. σ_P also depends on the distance d_i of the point from the nearest point actually assigned to the plane $\mathbf{P}_i$:

$$\sigma_P = \sqrt{\left[\sigma_Z \cdot \cot(\delta)\right]^2 + d_i^2} \qquad (6)$$

For small δ, we limit σ_P by a threshold σ_{Pmax}. If all vertices of $p_{i,j,k}$ are found to be incident with the intersection line $\mathbf{L}^{3D}$, $p_{i,j,k}$

is classified as an intersection. If $p_{i,j,k}$ is an outer boundary or if no vertex is found to be on $\mathbf{L}^{3D}$, $p_{i,j,k}$ is classified as a step edge. If some vertices of $p_{i,j,k}$ are determined to be on $\mathbf{L}^{3D}$ and others are not, $p_{i,j,k}$ will be split up into several new segments, each having a different classification. Of these new segments, any segment smaller than $2 \cdot \Delta$ and intersection segments whose average distance from the approximate polygon is larger than the segment length are discarded.
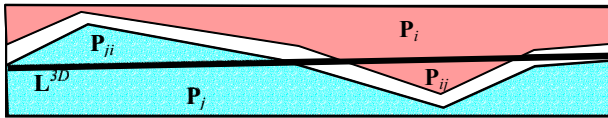

Figure 2.   Two planes $\mathbf{P}_i$, $\mathbf{P}_j$. $\mathbf{P}_{ij}$ is cut off $\mathbf{P}_i$ by intersection line $\mathbf{L}^{3D}$, and $\mathbf{P}_{ji}$ is the part of $\mathbf{P}_j$ cut off by $\mathbf{L}^{3D}$.
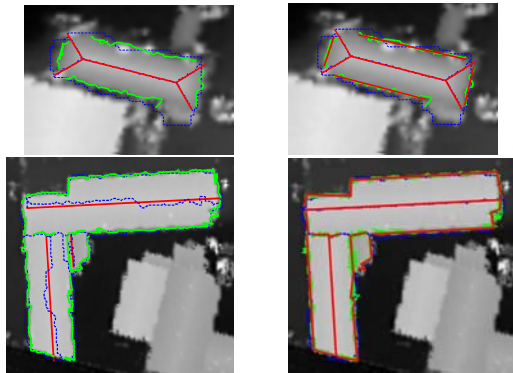

Figure 3.   Blue dashed lines: approximate boundary polygons. Green: original step edges. Red: final polygon segments. Left: before generalisation of step edges. Right: after improving the planar segmentation.

A further consistency check is carried out for intersection segments. The planimetric positions of the boundaries between neighbouring roof planes are very uncertain especially with flat roofs. In the lower building of figure 1, the roof planes have a tilt of about 2°, and the initial boundaries are about 2.5 m from the intersection line. Replacing the original boundaries by the intersection line will cause many points originally assigned to plane $\mathbf{P}_i$ to be within the boundary of $\mathbf{P}_j$ and vice versa (figure 2). Therefore, we compute the planar parameters of the cut-off segments $\mathbf{P}_{ij}$ and $\mathbf{P}_{ji}$. If $\mathbf{P}_{ji}$ is co-planar with $\mathbf{P}_i \setminus \mathbf{P}_{ij}$ (i.e. $\mathbf{P}_i$ without the points belonging to $\mathbf{P}_{ji}$) and if $\mathbf{P}_{ij}$ is co-planar with $\mathbf{P}_j \setminus \mathbf{P}_{ji}$, then the hypothesis that $\mathbf{L}^{3D}$ is the boundary between $\mathbf{P}_i$ and $\mathbf{P}_j$ is accepted; otherwise, a step edge is assumed. The left part of figure 3 shows the results of the classification of the segments $p_{i,j,k}$ for the two buildings in figure 1.

3.3   Detection of Step Edges

3.3.1   Detection of Candidate Points: Step edges correspond to the positions of maximum height changes. However, this is only true where no other objects interfere with the roof planes. That is why we include knowledge about the nature of roof planes into the extraction process. This process is different for step edges at outer boundaries and those separating two roof planes (figure 4). The original polygons $p_{i,j,k}$ are sampled at Δ. For each vertex of $p_{i,j,k}$, we try to determine one edge candidate point by analysing a profile of the DSM that is orthogonal to $p_{i,j,k}$ and passes through that vertex. The profiles should be long enough to make sure that they partly cover $\mathbf{P}_i$. All profiles are ordered from the interior of $\mathbf{P}_i$ to its exterior.
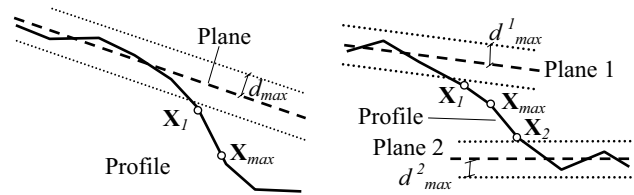

Figure 4.   Left: Step edge detection at building outlines. $\mathbf{X}_1$: the first point on the profile outside the tolerance band of width d_{max}. $\mathbf{X}_{max}$: point of maximum height gradient. Right: a step edge between two planes. $\mathbf{X}_1$ and $\mathbf{X}_2$: the first points outside the tolerance bands.

At outer boundaries, we look for the first point on the profile that is not on the plane $\mathbf{P}_i$, i.e. for the first point $\mathbf{X}_1$ having a distance larger than d_{max} (cf. equation 5) from $\mathbf{P}_i$. If no such point is found, the profile is supposed not to contain the step edge. Otherwise, the point $\mathbf{X}_{max}$ of maximum height difference is searched for on the profile starting from $\mathbf{X}_1$. The height difference between neighbouring points must be negative, because the terrain has to be lower than the roof. The search for a maximum is thus stopped if the height difference becomes positive, which happens if the roof boundary is occluded by a high tree. A further criterion is that the point $\mathbf{X}_{max}$ must be below the roof plane, otherwise it is discarded. By this criterion we eliminate points on low vegetation next to a roof. Where no candidate point is found, the step edge is thus assumed to be a straight line between the two closest step edge points visible to the sensor, which is exactly what a human operator would do in such a situation. For instance, in the upper building of figure 3, all corners are close to and partly occluded by trees. Building detection has included the group of trees in the right lower corner to the building. No incorrect edge points are determined.

With step edges separating two roof planes, we search for the first points $\mathbf{X}_1$ and $\mathbf{X}_2$ that are inconsistent with the two planes in a similar way. If the order of $\mathbf{X}_1$ and $\mathbf{X}_2$ is reversed, no step edge point can be determined; otherwise the position $\mathbf{X}_{max}$ of the step edge is determined as the position of the maximum height difference between $\mathbf{X}_1$ and $\mathbf{X}_2$.

3.3.2   Step Edge Generalisation: The detected edge polygons appear very noisy (figure 3) and need to be thinned out in a suitable manner. Again, we will mostly rely on statistical tests. However, we require one user-specified threshold which describes a degree of generalisation: the maximum length l_{max} of a polygon segment that can be discarded. We chose l_{max} to be 2 m and thus about two times the original point distance. First we eliminate points having a distance larger than l_{max} from both their predecessor and successor in the edge pixel chain. These outliers occur at profiles that belong to short segments of $p_{i,j,k}$ corresponding to noise. The remaining edge pixel chain is split into 2D segments $\mathbf{L}^{2D}_n$ by a simple recursive splitting algorithm. The parameters of $\mathbf{L}^{2D}_n$ are computed from an adjustment considering all edge points assigned to them. Segments containing less than three edge points are discarded. Then we test each pair of neighbouring 2D segments whether they are identical in the way described in section 2.3. We merge the pair possessing the best test statistic t_{L2DL2D} (equation 4) and recompute that test statistic for the neighbours of the merged segment. This procedure is repeated until no further segments can be merged. It turns out to be advantageous to replace the r.m.s. error of unit weight of the 2D segments by a fixed value equal to the original point spacing of the LIDAR data because the actual estimates

derived in the adjustment were too optimistic. We also consider segments with a combined r.m.s. error of unit weight smaller than Δ to be candidates for merging. In a second merging step we search for segments $\mathbf{L}^{2D}_n$ shorter than l_{max}. For those segments, we check whether their neighbours $\mathbf{L}^{2D}_{n-1}$ and $\mathbf{L}^{2D}_{n+1}$ are identical. If this is the case, $\mathbf{L}^{2D}_n$ is eliminated, and $\mathbf{L}^{2D}_{n-1}$ and $\mathbf{L}^{2D}_{n+1}$ are merged. Finally, the vertices of the polygon segment corresponding to the step edge are determined by intersecting neighbouring 2D segments. If the segments are nearly parallel, replacing the segment endpoints by the intersection point would change the direction one of these segments. If this is the case, or if more than 30% of one segment were cut off by the intersection, the neighbouring end points are connected by a polygon edge.

3.3.3 Improving the Planar Segmentation

3.3.3 Improving the Planar Segmentation: Now that the step edges have been determined precisely, the roof polygons p_i are obtained independently by a concatenation of their respective segments. The polygons are shifted with respect to their original positions. This affects the original segmentation and thus also the neighbourhood relations. That is why, after generating the roof polygons p_i, all pixels inside p_i assigned to a plane other than $\mathbf{P}_i$ and all pixels assigned to $\mathbf{P}_i$ outside p_i are eliminated from their respective planes. This is followed by a new iteration of region growing, where first the regions are only allowed to grow within their polygons p_i. Thus an improved segmentation is obtained. Small segments such as the plane $\mathbf{P}_f$ in figure 1 might be eliminated in this process. Having improved the segmentation, the boundary classification and step edge detection are repeated. The right part of figure 3 shows the final positions of all segments $p_{i,j,k}$ for the buildings in figure 1.

3.4 Combination of Roof Polygon Sections

Until now, all polygon segments $p_{i,j,k}$ were handled individually. Therefore, having determined the positions of these segments, consistency checks have to be carried out. First, the internal consistency of each polygon p_i is checked. If there are two consecutive segments $p_{i,j,k}$ and $p_{i,l,k+1}$ classified as intersections, we have to check whether the corresponding intersection lines themselves intersect. If replacing the segment endpoints $\mathbf{X}_{2,k}$ and $\mathbf{X}_{1,k+1}$ by the intersection point $\mathbf{I}$ changes the direction of one of the segments, a new step edge has to be inserted between $\mathbf{X}_{2,k}$ and $\mathbf{X}_{1,k+1}$ (figure 5). Second, we have to ensure that for each segment $p_{i,j,k}$ belonging to the boundary of plane $\mathbf{P}_i$, but not to the building outline, there is a matching opposite segment $p_{j,i,l}$ of the same type belonging to plane $\mathbf{P}_j$. If no such segment is found, it has to be inserted. With step edges, the 2D segments making up $p_{i,j,k}$ and $p_{j,i,l}$ have to be matched. We evaluate two measures between two 2D segments $\mathbf{L}^{2D}_m \in p_{i,j,k}$ and $\mathbf{L}^{2D}_n \in p_{j,i,l}$: the test statistic t_{mn} (equation 4) and the overlaps between the segments, i.e. the lengths of the projections of $\mathbf{L}^{2D}_m$ to $\mathbf{L}^{2D}_n$ and vice versa. We determine that $\mathbf{L}^{2D}_m$ and $\mathbf{L}^{2D}_n$ match if the overlap is more than 50% for one of the segments and if a statistical test shows the 2D lines to be identical. Edge pixel chains of matching segments are merged. Segments without a match are discarded.
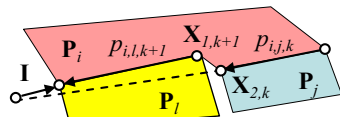

Figure 5. Checking consistency of $p_{i,j,k}$ and $p_{i,l,k+1}$

Having obtained consistency of the polygon segments both within their polygons and with respect to their neighbouring planes, the polygon segments have to be combined. This involves an adjustment of the vertices $\mathbf{X}$ at the transitions between consecutive polygon segments $p_{i,j,k}$ and $p_{i,j,k+1}$. First, all polygon segments intersecting at one planimetric position have to be found. Figure 6 shows an example involving three planes of which two intersect. There are altogether three polygon segments. One of them is the intersection line $\mathbf{L}^{3D}$, and the other two are step edges. Of the polygon segments corresponding to the step edges, the two 2D segments $\mathbf{L}^{2D}_{13}$ and $\mathbf{L}^{2D}_{23}$ closest to the intersection point are considered. There are two intersection points $\mathbf{X}_1$ and $\mathbf{X}_2$ having the same planimetric position but different heights. For adjustment, we consider all the planes in the vicinity of the vertices $\mathbf{X}_1$ and $\mathbf{X}_2$, i.e. the roof planes ($\mathbf{P}_1$, $\mathbf{P}_2$, $\mathbf{P}_3$) and the walls corresponding to the step edge segments ($\mathbf{L}^{2D}_{13}$, $\mathbf{L}^{2D}_{13}$). For each plane, we observe the distance between the plane and the point $\mathbf{X}_i = (X,Y,Z_i)$ to be 0. In order to model the uncertainty of the planes and step edges, we introduce approximate values $\mathbf{X}^0_i = (X^0,Y^0,Z^0_i)$ and compute the weights of the distance observations from the standard deviations σ_i of the distances between the approximate position $\mathbf{X}^0_i$ and the respective plane. The observation equations for a roof plane u giving support to height Z_i and for a wall w look as follows:

$$0 + v_{ui} = A_u \cdot (X^0 + \delta X) + B_u \cdot (Y^0 + \delta Y) + C_u \cdot (Z^0_i + \delta Z_i) + W_u;$$
$$0 + v_w = A_w \cdot (X^0 + \delta X) + B_w \cdot (Y^0 + \delta Y) + W_w; \qquad (7)$$
$$\sigma^2_{ui} = \mathbf{X}^{0T} \cdot \mathbf{Q}_{Pu} \cdot \mathbf{X}^0; \qquad \sigma^2_w = (X^0, Y^0) \cdot \mathbf{Q}_{Lw} \cdot (X^0, Y^0)^T$$

In equations 7, v denotes the correction of the observation. Equations 7 are used in an iterative least squares adjustment. After each iteration, the approximate co-ordinates are improved by the estimates $(\delta X, \delta Y, \delta Z_i)$,
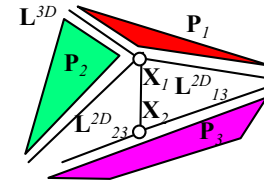

Figure 6. Vertex adjustment.

and the weights are re-computed. This model assumes that all walls intersect in one vertical line. Due to errors in step edge extraction, small step edge segments might have been missed and the extracted step edge segment might pass by the intersection point at (X,Y). To find such segments, we compute the normalised corrections $v^n_w = v_w / \sigma_w$ of the wall observations after each iteration and exclude the wall with a maximum value of v^n_w if $v^n_w > 3.5$. For all excluded walls, a new step edge segment is introduced between the original end point of the step edge and the adjusted position of the vertex. The left part of figure 7 shows the resulting roof boundaries.

3.5 Regularisation and Adjustment

After the vertices have been adjusted, a consistent polyhedral model in boundary representation is created. Only local information was used for the adjustment of the vertices. In an overall adjustment, all observations (original LIDAR points, 2D positions of step edges) should be used to determine the parameters of all planes and vertices simultaneously. The model can then be checked for geometrical regularities. Where evidence for such regularities is found, they can be considered in a final adjustment. In (Rottensteiner, 2003) we have presented the adjustment model and the way such regularities can be considered. The adjustment module has been implemented but has not yet been integrated into the algorithm. The "constraint generator" checking for geometric regularities has not yet been implemented. The right part of figure 7 shows

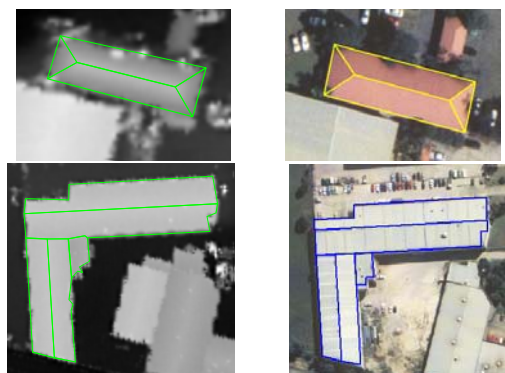the adjusted roof polygons with manually added constraints back-projected to an areal image of the area.

Figure 7.   Left: roof polygons after adjustment of vertices. Right: after overall adjustment with constraints (colours selected for visibility).
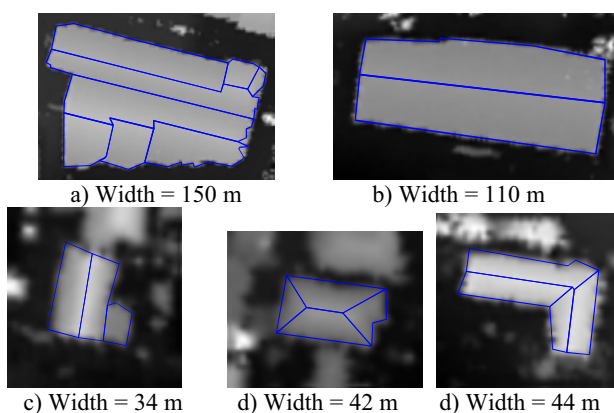

a) Width = 150 m   b) Width = 110 m

c) Width = 34 m   d) Width = 42 m   d) Width = 44 m

Figure 8. Five buildings extracted from the LIDAR data.

4.   RESULTS AND DISCUSSION

Figures 7 and 8 show some buildings extracted from the LIDAR data in our test data set. In general, the roof structure is well preserved in the models. Corners are not forced to be right-angled. The outline of the buildings still looks a bit ragged, and in some cases as in figure 8c the regularisation would improve the extracted model considerably. Figure 8d shows the limits of the plane extraction method: even though the general roof shape has been captured, the rightmost plane actually merges a smaller protruding building part consisting of two planes; the larger of these planes has 6 LIDAR hits, the smaller one has none. The industrial (lower) building in figure 7 is in general correctly reconstructed; however, an outlier in the LIDAR data caused a "hole" in the DSM which resulted in one of the corners on the right edge of the building being cut off. Figure 7 shows how the visual appearance is improved by the regularisation and the overall adjustment. The basis for such an adjustment is a topologically correct model, which can be systematically scanned for geometrical regularities. The industrial buildings in our examples (lower part of figure 7, figures 8a and 8b) are not easily reconstructed by primitives having a rectangular footprint. The r.m.s. error of planar fit is in the range of ±5 cm to ±10 cm for all planes. The inner accuracy of the adjusted building vertices in figure 7 is in the range of ±5 cm to ±30 cm in planimetry (depending on the intersection geometry, the geometric constraints, and the number of detected edge pixels for step edges) and ±2 cm to ±3 cm in height.

5.   CONCLUSIONS

We have presented a method for roof plane delineation from LIDAR data that aims at the reconstruction of buildings by polyhedral models. No 2D GIS data were required, and our examples show that models of a high level of detail can be reconstructed. Our method includes a new approach to step edge detection which should make the determination of building outlines less vulnerable to effects of adjoining trees. In the reconstruction process, most decisions are taken based on statistical tests or robust estimation, which is an important step towards making the reconstruction of buildings from LIDAR data more robust. The resulting building models are topologically correct if not yet regularised. Preliminary results using geometric constraints generated manually, based on visual inspection, show that using our method it is feasible to generate high-quality building models from LIDAR data alone.

REFERENCES

Alharty, A., Bethel, J., 2004. Detailed building reconstruction from airborne laser data using a moving surface method. In: *IAPRSIS* XXXV - B3, pp. 213-218.

Brenner, C., 2000. Dreidimensionale Gebäuderekonstruktion aus digitalen Oberflächenmodellen und Grundrissen. PhD thesis, University of Stuttgart. DGK-C 530.

Heuel, S., 2004. *Uncertain Projective Geometry. Statistical Reasoning for Polyhedral Object Reconstruction*. Springer-Verlag, Berlin Heidelberg, Germany.

Jiang, X., Bunke, H., 1999. Edge detection in range images based on scan line approximation. *Computer Vision and Image Understanding* 73(2), pp. 183-199.

Kager, H., 1989. ORIENT: A Universal Photogrammetric Adjustment System. In: A. Grün and H. Kahmen (eds), Optical 3-D Measurement, pp. 447–455.

Rottensteiner, F., 2003. Automatic generation of high-quality building models from Lidar data. *IEEE CG&A* 23(6), pp. 42-51.

Rottensteiner, F., Trinder, J., Clode, S., and Kubik, K., 2004. Using the Dempster Shafer method for the fusion of LIDAR data and multi-spectral images for building detection. *Information Fusion*. In print.

Sze, C.-J.., Mark Liao, H.-Y., Hung, H.-L., Fan, K.-C., Hsieh, J.-W., 1998. Multiscale edge detection on range images via normal changes. *IEEE TCAS-II* 45(8), pp. 1087-1092.

Vögtle, T., Steinle, E., 2000. 3D modelling of buildings using laser scanning and spectral information. In: *IAPRSIS* XXXIII-B3, pp. 927-933.

Vosselman, G., 1999. Building reconstruction using planar faces in very high density height data. In: *IAPRS* XXXII/3-2W5, pp. 87–92.